Two stochastic processes shape diverse senescence patterns in a single-cell organism

Ulrich K. Steiner*[1,2,3,4], Adam Lenart[1‡], Ming Ni[3,4,5‡], Peipei Chen[3,6], Xiaohu Song[3], François Taddei[3,4], Ariel B. Lindner[3,4†], & James W. Vaupel[1†]

[1] Max-Planck Odense Centre on the Biodemography of Aging, Campusvej 55, 5230 Odense, Denmark

[2]Biology Department, University of Southern Denmark, Campusvej 55, 5230 Odense, Denmark

[3]Center for Research and Interdisciplinarity, Paris Descartes University, 75014, Paris, France

[4]INSERM U1001, 75014 Paris, France

[5] Current address: BGI Shenzhen, Shenzhen, China

[6] Current address: National Center for Nanoscience and Technology, Beijing, China

Contributions

U.K.S. planned, performed, analyzed, and directed the experiments, and prepared and finalized drafts of the manuscript; M.N., performed experiments; A.L., X.S. analyzed data; F.T., A.B.L., J.V. and all other authors discussed the results and wrote the manuscript.

Competing financial interests

The authors declare no competing financial interests.

***Corresponding author: usteiner@biology.sdu.dk**

[†]Joint senior authors

[‡]Equal contribution of second authors

Abstract

Despite advancements in aging research, we lack basic understanding of the biological processes that shape senescence. Here, we show that for a simple isogenic bacterial system, *Escherichia coli*, in a controlled environment, senescence results from two stochastic processes: a primary random deterioration process within the cell underlying classical senescence patterns; and a secondary process of stochastic asymmetric transmission of a factor influencing mortality at cell fission. This second process is required to explain the near non-senescence of old mothers offspring and the lack of a mother offspring correlation in age at death. We observed that life span is predominantly determined by underlying stochastic stage dynamics. Our findings do not support evolutionary postulates that base their reasoning on the age-specific action of alleles, but could support stage-specific actions of alleles.

One Sentence Summary: Senescence in bacteria is driven by two stochastic processes that produce large variation in lifespan among isogenic individuals.

Main

One of the major challenges for biodemographic and aging research is to understand what drives senescence patterns *(1, 2)*. This challenge is not only illustrated by the variety of aging models that assume different generating processes for which we seek empirical evidence *(3–5)*, but also by an extensive literature on mechanistic approaches *(2)*. These approaches identify a multitude of underlying biochemical, molecular and organismal mechanisms that relate to the decline of function with age, many of which are rooted in direct or indirect oxidative processes *(2, 3)*. Examples include age-related mitochondrial dysfunction, telomere shortening, stem cell exhaustion, genotypic instability, epigenetic alterations, accumulation of damaged proteins and general loss of proteostasis *(2, 6, 7)*. Yet,

researchers have not conclusively determined whether such mechanisms are a cause or consequence of aging. This failure may be due to the complexity of model systems of aging. As a consequence, it is difficult to relate these mechanisms directly to the observed demographic patterns *(2, 6, 8)*. Only such linkage – between mechanisms and senescence patterns – can elucidate generating processes that underlie the various theories and aspects of aging.

Here, we quantify demographic parameters of a simple biological system, isogenic individual *E. coli* cells, under highly controlled environmental conditions. We used a high-throughput microfluidic device (Fig. S1; movie S1) to track individual cells throughout their lives *(9)*. Two types of cells were tracked: early daughter cells, offspring of young mothers, and late daughter cells, offspring of old mothers. A late daughter cell is the last daughter cell produced by an early daughter. That is, the early daughter cells are the mothers of the late daughter cells. We expect early daughters to hold little or no deterioration or damage at birth, whereas late daughters are likely be born with some damage. In this study, we use damage as a synonym for any unknown aging factor that leads to deterioration and increased mortality. We use this synonym because many aging factors are assumed to be accumulated damage caused by oxidative processes *(2, 10)*. A third group of cells, resembling the late daughter type are the last daughter cells produced by the late daughters, which we call second generation late daughters (Results only in SI).

In our experiments, we reveal classical senescence patterns of a decrease in reproduction (Fig. 1A, B) – indicated by decreased cell elongation and increased size at division with age (Fig. S3, Table S1) – for both early and late daughters (Figure 1A & B).

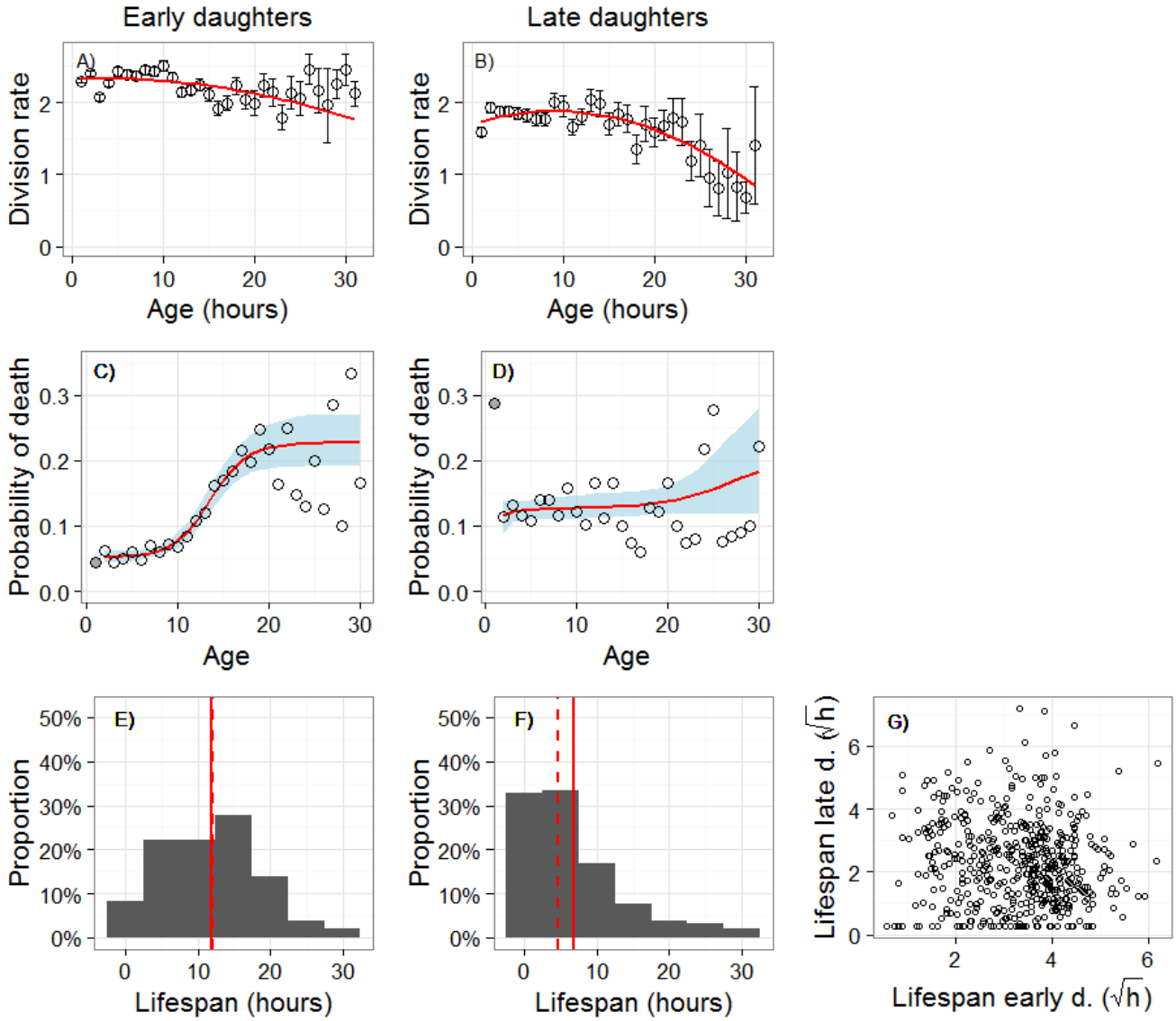

Fig 1: Division rate (divisions per hour) (A, B) and probability of death per hour (C, D) with increasing age, as well as lifespan distribution (in hours) (E, F) of isogenic *E. coli* cells grown under highly controlled environmental conditions in a microfluidic device (Fig. S1, Movie S1). Founding early daughter cells (A, C, E; N=516), and late daughter cells (B, D, F; N=516), the latter are the last offspring of the founding early daughters. Correlation of early daughter cells lifespan (mothers lifespan) (square root transformed for better visibility; N=516) versus the lifespan of their last daughter cell (late daughter cells; N=516) (G). For (A, B) means ± standard errors are plotted, for (C, D) means ± 95% confidence intervals are plotted. Red lines are models selected based on information criteria

(AIC) for (A, B) or likelihood optimization for Gamma-Gompertz-Makeham functions (C, D, see also Fig. 2, simulations below, and SI; Table S1-S2). For (E, F), mean and median are marked by solid and dashed lines respectively. For patterns of the second generation late daughters, see Table S2-4, and Fig. S4, S8-S12.

Our senescence patterns (Fig. 1 C, D) describe chronological aging in *E. coli* and support previous studies on replicative senescence (time counted as number of divisions) in this species *(11, 12)* (Fig. S3 & S5). Our main result highlights that early daughters and late daughters differ fundamentally in their senescence pattern, even though they are isogenic and grown in a highly controlled environment. Only the early daughters exhibit the classical senescence pattern, marked by an early exponential increase of the probability of death, followed by a later age mortality plateau. Late daughters have the same probability of death across most of their lives. Only late in life does mortality increase, but this increase is largely driven by only one data point, the one for the last age class (>30h). Such a plateau, exhibited by the early daughters – which is found in many higher organisms including humans *(1)* – has not been shown for bacteria before and might indicate deep-rooted features of aging and senescence. In yeast, ambiguous results on senescence patterns have been described *(8, 13)*.

We show that late daughter cells exhibit higher mortality than early daughter cells, except at very old age. Mortality in late daughters does not increase with age over most of their lives, i.e. no senescence is observed at the population level. The early age probability of death of late daughter cells (<=1hour, filled grey data point in Fig. 1D) equals that of the old age mortality plateau of early daughters (Fig. 1C; late daughter [<=1hour] q_x=0.19±0.04 mean±Std.Err.; see also the second generation late daughters, Fig. S4 q_x=0.23±0.05, early daughter Fig. 1C [>19 hours], q_x=0.20±0.02). The probability of death of newborn late daughters (<=1hour) drops after the first hour to a level that is lower than their

long-lived mothers (early daughters) and then remains at that level throughout their lives. This suggests a damage purging effect (see below). Such a drop of mortality after birth might indicate heterogeneity among newborns which selection acts upon *(14)*, e.g. heterogeneity in maternally-transmitted damage between mothers and daughters.

If we assume, as in most physiological theories of aging, that accumulated damage is the determining factor for the probability of death, then our observed constant probability of death with age (Fig. 1C, D) indicates an equilibrium distribution of damage among individuals. Such equilibrium is realized at the population level but not the individual level. It equilibrates on the one hand the accumulation of new damage within individuals (random cell deterioration), and on the other hand, the intracellular repair of damage and purging of damage by two mechanisms. The first mechanism reduces damage within an individual by asymmetric division of damage at cell fission, which increases variance in damage among individuals (mother and daughters). The second mechanism selects against highly damaged cells, i.e. the most damaged cells of a population die, which lowers the average level of damage in the population, and reduces the variance of damage among individuals *(15)*. Intriguingly, for our bacteria this equilibrium (plateau level) is significantly lower for late daughter cells (Fig. 1D, see Table S3) than the late-age mortality plateau of the early daughters (Fig. 1C). This indicates – based on fixed frailty models *(16)* – higher heterogeneity in transmitted damage of late daughters compared to early daughters. Such increased heterogeneity at birth predicts an earlier onset of selection against highly damaged cells which would explain why late daughters have on average less damage compared to early daughters at the plateau (see Fig. 2A, B, Fig. S11). Purging of damage through asymmetric division at cell fission has been shown in yeast, where late daughters showed reduced lifespan, but through further division and presumably damage dilution, the descendants of these late daughter yeast cells recovered

high longevity *(17)*. This is also reminiscent of asymmetric partition of protein aggregates in bacterial cells due to their passive accumulation in bacterial mother cells *(11, 18)*, though a causal link to senescence has yet to be established.

Further investigating our results in the light of the asymmetric transmission of damage between mothers and daughters, we were surprised not to find any influence of the lifespan of the mothers on the lifespan of their (last) daughters (Fig. 1G) (Table S6, Fig. S9). This result is remarkable given heritability of lifespan in humans and other complex organisms *(19)*. Furthermore, late daughters receive maternally transmitted damage that raises their probability of death from birth onwards. Early daughters seem to hold little or no damage, since their mothers have not yet accumulated much damage, whereas the average late daughter is born with some damage that raises its probability of death.

The lack of correlation between mother-daughter lifespan suggests that the mother-daughter transmission of damage is predominantly stochastic. Mothers that live long and might have accumulated more damage during their long life course do not transmit more damage to their daughters than do short-lived mothers (Fig. 1G). Short-lived mothers, which may have accumulated damage at a high rate, do not produce daughters with longer or shorter life expectancy. Our observation that early daughters – which hold little or no damage at birth – die at very different ages indicates that the accumulation of damage during the life course appears to be stochastic and varies highly among individuals. Despite the highly controlled environment in the microfluidic system and the isogenic cells, we observed a high variation in lifespan and reproduction among individuals, both for early daughters (Median±stdev lifespan 12 ± 7 hours, Coefficient of Variation, CV 0.57, Fig. 1E) (Fig. S8)

and late daughters (5± 7; CV=1.01, Fig. 1F). Such high variation supports substantial influences of stochastic events in shaping lifespan.

To support our conclusions based on the empirical results and to gain a better understanding of the underlying stochastic processes that shape our observed senescence patterns, we extended random deterioration process models which we describe in detail in the SI *(14, 15, 20)*. Our extended model assumes that early daughters are born without damage (Fig. 2A). With increasing age population level damage (and variance) slowly increases at early ages, accelerates after 10 hours and plateaus after 20 hours (Fig. 2A). These patterns in damage accumulation mirror the observed mortality patterns (Fig. 1C). Mortality plateaus, as observed for early daughters, can be explained by either fixed frailty, i.e. heterogeneity in damage stage at birth, or acquired heterogeneity throughout life *(14, 16, 21, 22)*. In our system heterogeneity in damage stage at birth has little influence, at least for early daughter cells. Senescence is driven by the baseline mortality and accrued damage as in random deterioration models *(14, 20, 21)*. This conclusion is supported by two results of our model. First, most early daughters die with no or very little damage (Fig. S11), and second, the observed survival patterns follow closely the survival curve of simulated cells that did not accumulate any damage throughout life (Fig. 2C).

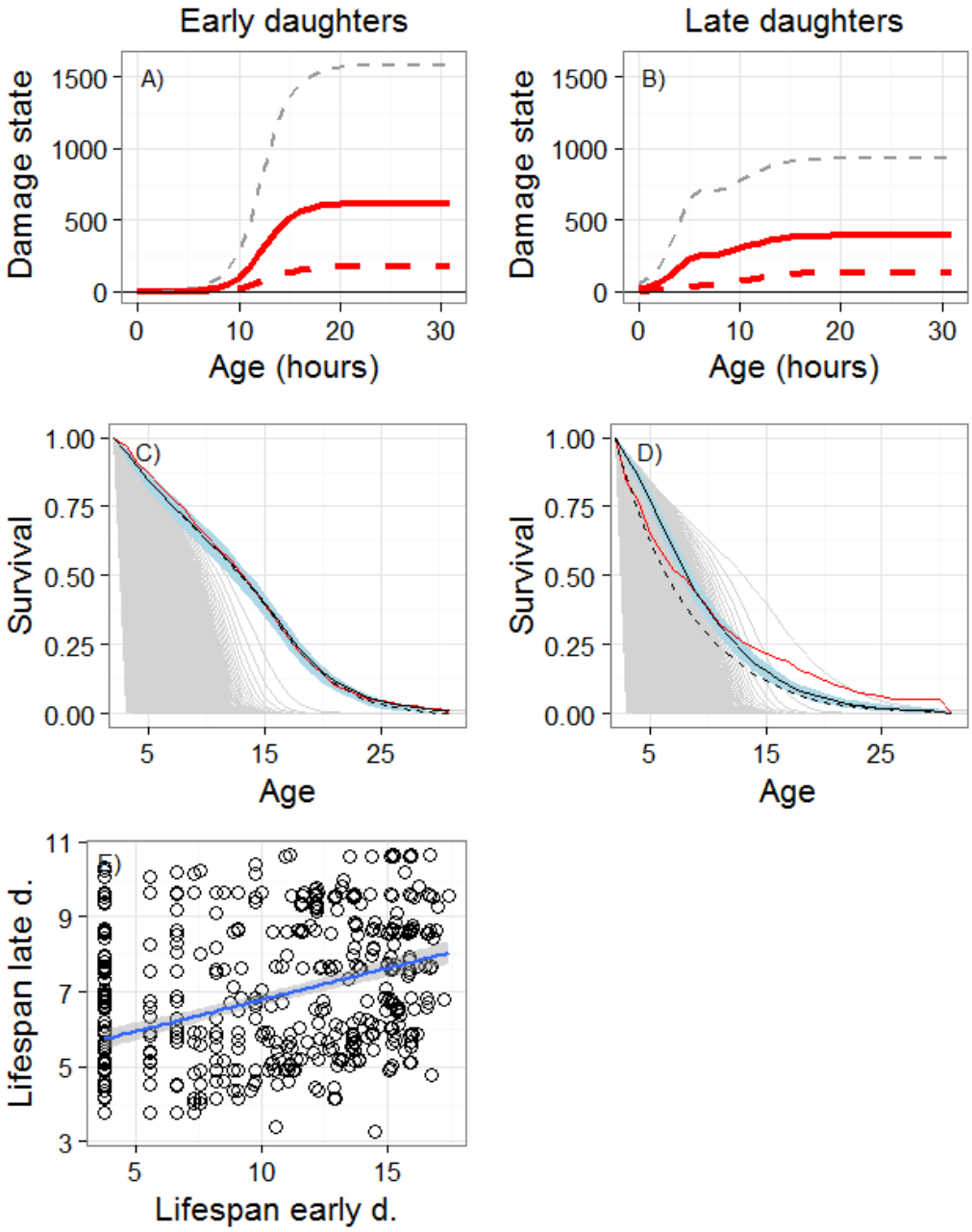

Fig. 2: Mean (red solid line, + SD grey hatched lines) and median (red hatched line) damage state with increasing age (A, B); observed experimental population level survival curve (red solid line; see also related probability of death Fig. 1 C, D), Gamma-Gompertz-Makeham simulated survival curve with symmetric damage transmission (hatched black line) as well as asymmetric damage transmission of 7%

(solid black line ± 95% CI in blue) (C, D). Graphs are shown for early daughter cells (A, C) and late daughter cells (B, D). Thin grey lines in (C, D) depict expected survival curve of cells with different fixed damage state: outermost curve depicts the highest survival of cells with no damage throughout their lives, most left survival curve depicts the lowest survival of cells that were born with maximum damage level of 5000. Lifespan (square root transformed) of simulated 516 early daughter cells (mothers) versus the lifespan of their last daughter cell (late daughter cells) with 7% mother to daughter damage transmission (E). The blue line illustrates the correlation in lifespan between mothers and daughters (~0.25, with 95% CI in grey), given a fixed 7% mother to daughter damage transmission at cell fission.

Contrasting the early daughter cells, late daughters are born with some damage *(14)*(Fig. 2B). For the following results, it is important to note that this heterogeneity in damage at birth of late daughters is an underestimation since we do not include the exceptionally high first-hour mortality rate (grey filled data point in Fig. 1D) in the simulations. In our simulations the distribution of this damage at birth is related to the distribution of the accumulated damage at death of the early daughter cells (mothers of the late daughters, Fig. S11). For the simulations, we assumed that the mother to daughter transmission of damage is a fixed fraction of all the damage the mother accumulated over her lifespan. We determined this fraction at a surprisingly low level of 0.07, which indicates a highly asymmetric division of damage between mothers and daughters. If damage transmission between mothers and daughters would be symmetrical (0.5), the predicted survival of the simulations (Fig. 2D hatched line) does not match the observed survival (Fig. 2D red line). For early daughters, the level of asymmetry makes little difference because most of them die with no or little accumulated damage (Fig. 2C, Fig. S11). The predicted survival pattern of late daughters at older ages slowly converges to the simulated

survival patterns of undamaged cells (outer right grey line) (Fig. 2D). Therefore, many cells that survive to old ages hold little damage, which supports our interpretation of the empirical data that late daughter cells are born with diverse damage states, highly damaged cells are selected against, and at old ages, population-level survival patterns are strongly influenced by cells that have not accumulated much damage. Such selective effects have been described by population level demographic theories as heterogeneity's ruses, where selection among different damage stages (fixed frailty) leads to diverse senescence patterns at the population level *(22)*. Even though the optimized fixed transmission fraction between mother and daughters of our model is surprisingly low at 0.07, such a fixed fraction would lead to a correlation in lifespan between mother and daughters of about 0.25 (Fig. 2E fitted line). The observed data does not support such correlation in lifespan (Fig. 1G) and hence supports our conclusion that the fraction of transmitted accumulated damage from mother to daughter at cell fission varies stochastically and is not fixed at a low level of 0.07 as our model assumes.

In this study, our experimental setup limits our analysis to two extreme cases: early and late daughter cells (in fact the last daughter cells). We hypothesize that the results do not only hold for these two extremes but rather portray the extremes of a continuous process across different aged cells. Two observations support our claim: first, changes in mortality of early daughters (Fig. 1C) and age patterns in reproduction (Fig. 1A) are gradual, suggesting a gradual underlying mechanism; second, we do not observe a pronounced pattern just before death (Fig. S6 & S7). Such a pattern would be expected if the last daughters are exceptional because their mothers are approaching death, for instance in the way as predicted under terminal investment theories.

Our findings lead to the conclusion that the diverse senescence patterns, including the classical senescence pattern of a mortality plateau, are determined by two stochastic processes that relate to underlying (damage) states and only indirectly to age *(14, 15, 21, 23)*. The primary process is a random deterioration process, e.g. the stochastic accumulation of damage throughout life, and the secondary process involves the stochastic transmission of damage from the mother to their daughters at cell fission. This transmitted damage or some other unknown aging factor increases the probability of death but is non-heritable as we show by the lack of correlation between mother and daughter lifespan *(14, 15, 21, 23)*. Other commonly assumed drivers of senescence, such as age itself, the environment, epigenetic, or genetic variability can be ruled out in our study. If chronological age determined senescence, early and late daughter cells would show similar mortality patterns. The highly controlled microfluidic system creates a uniform environment and hence we can exclude extrinsic environmental drivers; this does not imply that senescence patterns do not differ under different environmental conditions. If epigenetic or genetic variability had a significant influence (even though we aimed at working with isoclonal individuals), a positive correlation among mother and daughter lifespan would be seen. Our findings indicate that two simple stochastic processes can create complex senescence patterns. The basic arguments behind evolutionary theories of aging, such as mutation accumulation and antagonistic pleiotropy theories, do not apply to this study*(4)*. This is not self-evident, since the logic behind such theories applies to single celled organisms as well as multicellular organisms; in both types of organisms evolutionary selective forces decline with increasing age. The substantial effect of stochastic events on life histories is also indicated by the large variability in life histories despite excluding any genetic or environmental variability. Such large stochastic variation supports arguments behind neutral theories of life history *(24)* that suggest that stochastic variability can account for substantial fractions of the total variability in fitness components. Our interpretation of stochastic

events determining individual life courses is consistent with findings of significant stochastic influences at the molecular *(25)* and protein level *(6, 26)* and adds to the growing interest in such phenotypic heterogeneity and individuality *(27–29)*. Our findings on stochastic characteristics are also consistent with long standing arguments about non-genetic and non-environmental individual heterogeneity being driven by low copy numbers of proteins *(30)*. Recent empirical evidence shows that such copy numbers follow a distribution*(31)* predicted by the demographic models on which our extended random deterioration models are rooted *(16)*.

Future challenges will include determining whether these stochastic processes are neutral or adaptive, and what drives their evolution *(32)*. For the basic aging processes that drive senescence, the causal relationships that drive age patterns are currently unknown. The complex senescence patterns found in this study of a simple model organism under highly controlled conditions emphasizes the challenges to quantify contributions of well-defined determinants of aging in the complex systems on which most aging research is focused *(2)*. In light of the growing evidence that stochastic processes can have cascading effects across all levels of higher organisms *(19, 25, 26)* new avenues in aging research may require a shift towards the underlying stochastic processes that drive such stage dynamics rather than focusing on age patterns itself, in simple systems like bacteria and perhaps beyond. Promising steps in such directions have been initiated by exploring stage-specific alleles shaping senescence patterns*(5)*.

Acknowledgements

We thank D.A. Roach, D. Steinsaltz, T. Coulson, and S. Tuljapurkar for discussions and comments. We were supported by the Max Planck Society and Marie-Curie PIEF-GA-2009-235205 (U.K.S), Axa

Foundation Chair for Longevity, Agence National de la Recherche, "Who am I?" Labex grant

Université Sorbonne Paris Cite.

References

1. J. W. Vaupel, J. R. Carey, K. Christensen, T. E. Johnson, A. I. Yashin, N. V Holm, I. A. Iachine, V. Kannisto, A. A. Khazaeli, P. Liedo, V. D. Longo, Y. Zeng, K. G. Manton, J. W. Curtsinger, Biodemographic trajectories of longevity., *Science (80-.).* **280**, 855–60 (1998).

2. C. López-Otín, M. A. Blasco, L. Partridge, M. Serrano, G. Kroemer, The hallmarks of aging., *Cell* **153**, 1194–217 (2013).

3. T. B. L. Kirkwood, Understanding the odd science of aging., *Cell* **120**, 437–47 (2005).

4. W. D. Hamilton, The moulding of senescence by natural selection, *J. Theor. Biol.* **12**, 12–45 (1966).

5. K. W. Wachter, D. Steinsaltz, S. N. Evans, Evolutionary shaping of demographic schedules., *Proc. Natl. Acad. Sci. U. S. A.* **111 Suppl**, 10846–53 (2014).

6. J. Tyedmers, A. Mogk, B. Bukau, Cellular strategies for controlling protein aggregation, *Nat. Rev. Mol. cell Biol.* **11**, 777–788 (2010).

7. A. B. Lindner, A. Demarez, Protein aggregation as a paradigm of aging., *Biochim. Biophys. Acta* **1790**, 980–96 (2009).

8. A. Denoth Lippuner, T. Julou, Y. Barral, Budding yeast as a model organism to study the effects of age., *FEMS Microbiol. Rev.* **38**, 300–25 (2014).

9. F. Gasset-Rosa, A.-S. Coquel, M. Moreno-Del Álamo, P. Chen, X. Song, A. M. Serrano, M. E. Fernández-Tresguerres, S. Moreno-Díaz de la Espina, A. B. Lindner, R. Giraldo, Direct assessment in bacteria of prionoid propagation and phenotype selection by Hsp70 chaperone., *Mol. Microbiol.* **91**, 1070–87 (2014).

10. T. B. L. Kirkwood, M. Feder, C. E. Finch, C. Franceschi, A. Globerson, C. P. Klingenberg, K. LaMarco, S. Omholt, R. G. J. Westendorp, What accounts for the wide variation in life span of genetically identical organisms reared in a constant environment?, *Mech. Ageing Dev.* **126**, 439–443 (2005).

11. A. B. Lindner, R. Madden, A. Demarez, E. J. Stewart, F. Taddei, Asymmetric segregation of protein aggregates is associated with cellular aging and rejuvenation., *Proc. Natl. Acad. Sci. U. S. A.* **105**, 3076–81 (2008).

12. P. Wang, L. Robert, J. Pelletier, W. L. Dang, F. Taddei, A. Wright, S. Jun, Robust growth of Escherichia coli., *Curr. Biol.* **20**, 1099–103 (2010).

13. N. Minois, M. Frajnt, C. Wilson, J. W. Vaupel, Advances in measuring lifespan in the yeast Saccharomyces cerevisiae., *Proc. Natl. Acad. Sci. U. S. A.* **102**, 402–6 (2005).

14. A. I. Yashin, J. W. Vaupel, I. A. Iachine, A duality in aging: the equivalence of mortality models based on radically different concepts, *Mech. Ageing Dev.* **74**, 1–14 (1994).

15. S. N. Evans, D. Steinsaltz, Damage segregation at fissioning may increase growth rates: a superprocess model., *Theor. Popul. Biol.* **71**, 473–90 (2007).

16. T. I. Missov, J. W. Vaupel, Mortality Implications of Mortality Plateaus, *SIAM Rev.* **57**, 61–70 (2015).

17. B. K. Kennedy, Daughter cells of Saccharomyces cerevisiae from old mothers display a reduced life span, *J. Cell Biol.* **127**, 1985–1993 (1994).

18. A.-S. Coquel, J.-P. Jacob, M. Primet, A. Demarez, M. Dimiccoli, T. Julou, L. Moisan, A. B. Lindner, H. Berry, Localization of protein aggregation in Escherichia coli is governed by diffusion and nucleoid macromolecular crowding effect., *PLoS Comput. Biol.* **9**, e1003038 (2013).

19. C. Finch, T. B. Kirkwood, *Chance, Development, and Aging* (Oxford University Press, Oxford, 2000).

20. H. Le Bras, Lois de mortalité et age limite, *Population (Paris).* **33**, 655–691 (1976).

21. J. Weitz, H. Fraser, Explaining mortality rate plateaus, *Proc. Natl. Acad. Sci. U. S. A.* **98**, 15383–15386 (2001).

22. J. W. Vaupel, A. I. Yashin, Heterogeneity's Ruses: Some Surprising Effects of Selection on Population Dynamics, *Am. Stat.* **39**, 176 (1985).

23. K. W. Wachter, Evolutionary demographic models for mortality plateaus, *Proc. Natl. Acad. Sci.* **96**, 10544–10547 (1999).

24. U. K. Steiner, S. Tuljapurkar, Neutral theory for life histories and individual variability in fitness components., *Proc. Natl. Acad. Sci. U. S. A.* **109**, 4684–9 (2012).

25. M. B. Elowitz, A. J. Levine, E. D. Siggia, P. S. Swain, Stochastic gene expression in a single cell., *Science (80-.).* **297**, 1183–1186 (2002).

26. G. Balázsi, A. Van Oudenaarden, J. J. Collins, Cellular decision making and biological noise: from microbes to mammals., *Cell* **144**, 910–925 (2011).

27. M. Ackermann, A functional perspective on phenotypic heterogeneity in microorganisms, *Nat. Rev. Microbiol.* **13**, 497–508 (2015).

28. C. J. Davidson, M. G. Surette, Individuality in Bacteria, *Annu. Rev. Genet.* **42**, 253–268 (2008).

29. M. Wolf, G. S. van Doorn, O. Leimar, F. J. Weissing, Life-history trade-offs favour the evolution of animal personalities, *Nature* **447**, 581–584 (2007).

30. J. L. Spudich, D. E. Koshland, Non-genetic individuality: chance in the single cell, *Nature* **262**, 467–471 (1976).

31. Y. Taniguchi, P. J. Choi, G.-W. Li, H. Chen, M. Babu, J. Hearn, A. Emili, X. S. Xie, Quantifying E. coli Proteome and Transcriptome with Single-Molecule Sensitivity in Single Cells, *Science (80-.).* **329**, 533–538 (2010).

32. D. Steinsaltz, S. N. Evans, Markov mortality models: implications of quasistationarity and varying initial distributions., *Theor. Popul. Biol.* **65**, 319–37 (2004).

33. R. A. language and environment for statistical computing. R Core Team, R. D. C. Team, Ed. R: A language and environment for statistical computing.*R Found. Stat. Comput.* **1**, 409 (2016).

34. K. Burnham, D. R. Anderson, *Model selection and multimodel inference : a practical information-theoretic approach* (Springer, New York, Second., 1998).

35. F. R. Blattner, The Complete Genome Sequence of Escherichia coli K-12, *Science (80-.).* **277**, 1453–1462 (1997).

36. P. Jagers, in *Biomathematics and cell kinetics*, (Elsevier, Amsterdam, 1978), pp. 21–29.

37. H. Caswell, *Matrix population models: construction, analysis, and interpretation* (Sinauer Associates, 2001).

38. E. J. Stewart, R. Madden, G. Paul, F. Taddei, Aging and death in an organism that reproduces by morphologically symmetric division., *PLoS Biol.* **3**, e45 (2005).

39. M. Ackermann, S. C. Stearns, U. Jenal, Senescence in a bacterium with asymmetric division., *Science* **300**, 1920 (2003).

40. B. Charlesworth, *Evolution in age-structured populations* (Cambridge University Press, Cambridge, 1994).

41. T. Clutton-Brock, Reproductive effort and terminal investment in iteroparous animals, *Am. Nat.* **123**, 212–229 (1984).

42. G. Williams, Natural selection costs of reproduction and a refinement of Lacks principle, *Am. Nat.* **100** (1966).

43. K. Mattick, R. Rowbury, T. Humphrey, Morphological changes to Escherichia coli O157:H7, commensal E. coli and Salmonella spp in response to marginal growth conditions, with special reference to mildly stressing temperatures., *Sci. Prog.* **86**, 103–113 (2003).

Supplemental material

Methods

Summary of methods

We collected data in two independent sets of experiments. We loaded *E. coli* K12-derived MG1655 strain cells into the designed microfluidic (PDMS) chip *(9, 12)* from an exponentially growing culture in supplemented minimum media M9. During each experiment, we acquired 77 hours of time lapse phase-contrast imaging (15 frames/hour for each of the 2x44 fields followed) using a temperature-controlled (at 43°C) inverted microscope. The rod-shaped bacteria cells grew in dead end side channels of a microfluidic chip, with the focal cells trapped at the end of the side channels, and we tracked them over their lifespan (Fig. S1; movie S1). We used customized image analysis to generate the demographic data (lifespan, cell elongation rate, cell size, and time of each division).

We assured by starting the experiments with exponentially growing cells that the initial loaded cells are descendants of young mothers (i.e. they are early daughter cells) (Fig. S2). At the end of their lives, these early daughter cells produced a last daughter (late daughters) that then became the next bottom-most cell trapped at the end of the respective growth channel. Therefore we could directly compare mother and daughter cells. Note that the late daughters are not born at the same time (main text Fig. 1 E,F). The late daughter cells produced another generation of late daughter cells at the end of their lives (second generation late daughter cells) for which the results are shown in Fig. S3-9 & Table S1-3. Statistical analysis on the empirical data were done in program R *(33)* using general linear, generalized linear, and non-linear models. Models were selected based on information criteria (AIC) *(34)* or based on differential evolution algorithm for global optimization (R package DEoptim).

For the extended random deterioration model, we first estimated parameters by fitting a fixed frailty model – a Gamma-Gompertz-Makeham (GGM) model – to the observed survival data of the early daughter cells *(14, 16)*. We then translated these fitted GGM model parameters to an extended random deterioration process model, an extended LeBras type deterioration model *(20)*. In doing so, we took advantage of mathematical similarities between the two types of models, even though they are biologically distinct *(14, 16)*. With these random deterioration model parameters we could estimate the probability matrix of an individual being at stage *i* at age *x*. Microsimulations based on these models provided stage at death distribution. For the late daughters, we assumed that they are born at a scaled version of the same damage stage in which their mothers died. We also assumed that late daughters accumulate damage at the same rates as early daughters do, i.e. same probabilities to transition to a higher damage state of early and late daughters. We further assumed that the amount of accumulated damage in late daughters had the same effect on mortality than on early daughters, that is, early and late daughter cells are not fundamentally different except that late daughters are born in different damage stages, while early daughters start their lives without damage. Our model simplifies the biological system substantially in as much as no repair of damage or purging of damage through asymmetric division at cell fission is considered. Damage accumulates unidirectionally, mortality increases exponentially with accumulated damage, and each cell suffers from an age-independent baseline mortality risk (Makeham term).

Strains and growth conditions

We fabricated the microfluidics chips as previously described *(9)*. We grew *E. coli* K12 MG1655 *(35)* strain derivative (intC::pSulA-yfp) cells at 43°C in filtered minimal medium supplemented with 0.4% Glucose and 0.2% Casamino Acids (hereafter M9). We diluted 100µl of the overnight culture into 50ml

of M9 and then grew it at 43°C to exponential growth phase (OD600 ~0.2). We centrifuged the cells and resuspended the cell pellet in 100µl of M9 to load them into the chip by injection into the main (feeding) channel followed by centrifugation (15 minutes at ~168g). We applied a continuous laminar flow (2.7ml/h) of M9 supplemented with 1.5% Polyethylene Glycol (PEG P3015 Sigma Aldrich) through the main channel throughout the experiment. The temperature was kept constant at 43°C (see below).

Time-lapse imaging

We followed bacterial growth in the microfluidics chip by phase-contrast time-lapse imaging at a rate of 4min/frame using a MetaMorph (Molecular Devices)-controlled inverted Nikon microscope (Eclipse Ti, 100xobjective, CoolSNAP HQ2 camera) with a temperature-control chamber (Live Imaging Services). We continuously scanned 44 positions, each comprising 18 channels, for 77 hours, in two independent experimental sets.

Image analysis

We used a custom image analysis to segment all cells within the side channels per frame, the software measured the cells' location and size within the time series and generated cell lineages. To this end, phase contrast time-lapse images were lowpass-filtered and background flattened (MetaMorph Molecular Devices software) to increase contrast. We further processed the images by a customized ImageJ plugin for cell segmentation to crop each of the growth channels, stabilize the time sequenced images, adjust the brightness and to create a binary image by thresholding and filtering (median filter). Finally, the ImageJ plugin water-sheds the time sliced images. We then applied a final round of segmentation in Matlab by correcting errors in segmentation by checking for minimum (0.8) and

maximum (1.4) cell elongation rates for each cell (size time-4 min, size time+4min). This way, we recorded for any time points (at 4 minute intervals) the exact location of a cell in the side channel (the pixel coordinate of the center of mass of the cell area), the side channel of the cell, and if a cell divided. By the position within the side channel we determined which cell was the mother (old pole progenitor) cell (bottommost cell), their most recent daughter (new pole progenitor) cell and so forth. We measured the length of a cell as the largest distance of the rod shaped cell in the orientation of the side channel. We applied a minimum "cell length" of ~1µm to exclude artefacts originating mainly from small deformations in the growth channels, or some shadows/reflections generated at the dead end of the growth channel.

Age at death

We defined age at death as the time when a cell stopped growing and dividing for at least one hour and 20 min. None of the cells divided after such a long division arrest or resumed growth.

Early and late daughter cells

We defined the early daughter population as the cells that were initially loaded into the microfluidic chip and settled at the dead-end of the side channels. They originated largely from young mothers because the population was in exponential growth phase when we loaded cells into the chip *(36)*. The age distribution of these early daughter cells is, because of the exponential growth phase, negatively exponentially distributed. We show their expected age distribution in Fig. S2, based on a Leslie matrix generated from the survival and division rates of the early daughters (Fig. 1A & C). Due to the exponential growth phase, we assume a stable age distribution (the right eigenvector corresponding to the dominant eigenvalue of the Leslie matrix) *(37)*. We tracked these early daughter cells to the end of

their lives (Fig. S1, movie S1). The last daughters that were produced by these early daughter cells are the late daughter population. These late daughters are all of age zero but originate from mother cells (the early daughters) that had accumulated damage over their lives, and that were only one division from dying. We again tracked these late daughters throughout their lives. We focus mainly on these first two types of cells (early and late daughters), though as expected, the next generation of late daughter cells (second generation late daughters) follow the late daughter patterns (Fig. S5-7).

Estimating demographic parameters

Image analysis (see above) provided us the basis for estimating the age-specific demographic parameters: division rate, cell elongation rate, size at division, and survival rate. We excluded all cells that were not tracked throughout their lives. This concerned mostly cells that filamented (cell division arrested without growth arrest) and were flushed out of the side channels when they reached a size longer than 25 μm (length of the side channel). We also excluded all (early and late daughter) cells that died at chronological age 0 (never started to grow or divide). This was practiced because loading into the chip might be damaging and we wanted to exclude such death. This approach was conservative, because fewer early daughters never started growing or divided compared to late daughters (who could not have been damaged by the loading). We used data from 516 early daughters that produced 516 late daughters which in turns produced 298 (second generation) late daughters that were tracked throughout their lives.

Statistical analysis

We did the statistical analysis using the R software *(33)*. We estimated and plotted hourly rates, rather than rates on the 4 min intervals because data would be sparse for 4 min intervals at older ages. We

also clustered all data of ages beyond 30 h for the same reason. To guide our model selection *(34)*, we used AIC (Akaike Information Criteria) and considered better support between models when the ΔAIC was more than 2. For the parameter estimation of the GGM and extended random deterioration models, we used the DEoptim R package and the optim function within the stats R package. We calculated the CI (Fig. 1 C & D) by bootstrapping 1000 times.

Lifespan distribution second generation late daughters

In the main article, we focused on early and late daughter cells. Qualitatively, patterns of the second generation late daughters (the last daughters produced by the late daughters) correspond to those of their mothers (the late daughters), though data becomes sparse uncertainty increases and some deviations occur. Fig. S8 illustrates lifespan distributions of the 298 second generation late daughters, their mothers (late daughters), and grandmothers (early daughters). Kolmogorov-Smirnov tests (two-sided) verifies that both lifespan distributions between early and late daughters ($D = 0.3691$, $p < 0.00001$), and early to second generation late daughters are significantly different ($D = 0.4094$, $p < 0.00001$), while those between late daughters and second generation late daughters do not differ ($D = 0.0973$, $p = 0.1189$).

Heritability or cross generation correlation in lifespan

In order to estimate correlation of lifespan between mother cells (early daughters) and their last (late) daughter cells, we used linear models on square root transformed data for age at death (lifespan) for the mothers' lifespan as response variable and their last daughters' lifespan as explanatory variable, or intercept only models (null model) as comparative models.

Model selection (Table S6) does not allow distinguishing between the two alternative models and we cannot completely rule out that the longer-lived mothers produce slightly shorter- lived late daughters (Fig. 1G). In any case, the effect size is weak and such a negative correlation would suggest that longer-lived mothers accumulate more damage that is then partly transmitted to their late daughter. Similar results hold for late daughters to second generation late daughters (Fig. S9). We cannot completely rule out a weak tendency that long-lived (late daughter) mothers produce last daughters (second generation late daughters) that live slightly shorter (Table S6). In any case, our simulations with a low fixed transmission rate of 7% of damage transmitted between mother and daughters would lead to much higher correlation in lifespan as observed (Fig. 2E main text).

Lifespan and lifetime reproductive success: reproductive and chronological aging

Previous aging studies on *E. coli (12, 38)* and other bacteria *(39)* or many yeast studies *(8)* have focused on replicative aging and patterns have been described for time measured in number of divisions. Such age measures can be difficult to compare directly to chronological age if the time between divisions varies. Nonetheless, we detected a strong correlation between lifespan and the lifetime reproductive success (number of divisions an individual undergoes throughout its life), but there remains some variation, particularly for longer lived individuals (Fig. S5).

Division rate

We fitted linear models on hourly average division rates (at the cellular level) as response variable and age as explanatory variable. A model with a linear and quadratic term was best supported for the early (Fig. 1A), late (Fig. 1B) and second generation late (Fig. S4A) daughters (Table S2).

Mortality rate

We fitted Gamma-Gompertz-Makeham related models to the survival data. GGM models were tested for assumptions among parameters, for instance, whether shape and scale parameters are independent or defined by a rate parameter. For late (Fig. 1D) and second generation late daughters (Fig. S4B), we optimized the scaling of the mother to daughter state relationship (transmission factor) based on the age at death state distribution of early daughters (or late daughters for second generation late daughters) (Fig. S11). We assumed that accumulation of damage, which is the stage transition probabilities did not differ among early, late and second generation late daughters. We also assumed that the effect of the stage was not different for early, late or second-generation late daughters. These assumptions allowed us to use the translated GGM estimates of the early daughters also for late and second generation late daughters.

Difference in motrality rates at old ages for early and late daughters

The late age mortality plateau detected in early daughters (Fig. 1C) and the flat mortality hazard pattern of the late daughters might indicate similar mortality rates at older ages (>19 hours). To test for this we compared models that distinguished between early and late daughters but only included cells that survived to an age of at least 20 hours. Late daughter cells have lower mortality rates (qx=0.1248±0.0191 mean±Std.Err.) than early daughters at old ages (qx=0.2005±0.0168 mean±Std.Err.) (Table S3) . This result comprises 73 early daughters and 41 late daughters that lived longer than 19 hours.

Difference in mortality rates among old early daughters and newborn (first hour) late daughters and newborn second generation late daughters

Old age (>19 hours) early daughters show a mortality plateau at qx=0.20±0.02 mean±Std.Err., that does not differ from the first hour of late daughters‘ and second generation late daughters‘ mortality rate (late daughters: qx=0.19±0.04 mean±Std.Err.; second generation late daughters: qx=0.23±0.05 mean±Std.Err.; Pearson's Chi-squared testing: X-squared = 1.64, df = 2, p-value = 0.44; see also Fig. 1C, D and Fig. S4B). The Chi-squared test compares the 280 survival events and 73 death events of the early daughters (between age 19 and death of all early daughters) to the 416 late daughter cells that survived the first hour and the 100 late daughters that died within the first hour, and the 229 second generation late daughters that survived their first hour and the 69 second generation late daughters that died within their first hour of life.

Cell elongation rates

We fitted linear models for cell elongation rates for early, late and second generation late daughters. For all three cell types a model with a linear and quadratic term was best supported, though the curvature was minimal for early daughters (Table S1). Early and late daughters showing clear decline in cell elongation rate with age, while second generation late daughters first increase in cell elongation rate before levelling off and maybe declining at old ages (Fig. S3).

Size at division

We fitted linear models for cell size at division for early, late, and second generation late daughters. For all three cell types, a model with a linear and quadratic term was best supported, though the curvature was minimal for early and late daughters (Table S1). Early and late daughters showed clear senescence in cell elongation rate while the second-generation late daughters selected models might be over-fitted (Fig. S3).

Reverse time analyses: Hours before death

Chronological aging follows individuals from birth to death and time counted starts at birth. Various hypotheses about the evolution of life histories, aging and senescence, in particular, terminal investment strategies *(40–42)*, assume that individuals can sense that they are approaching death and that an optimal strategy for an individual might be to invest remaining resources into reproduction rather than maintenance when approaching immediate death. As Fig. 1 & 2 in the main text illustrates, age at death is highly variable, for that chronological senescence patterns and terminal investment strategies might provide very different insights. We investigated whether patterns in reproduction (division rate), cell elongation rate, or size at division differ significantly when time is counted backward (remaining lifespan), starting with death. We would expect that the last hour before death would show significant changes compared to the more spread out chronological senescence patterns (Fig. 1, Fig. S4 & S5). In general, there seems to be little evidence that terminal investment is happening to a larger degree, at least such strategies if existent, do not show larger effects compared to chronological aging and classical senescence (Fig. S6 & S7, Table S4 & S5).

Division rate for hours before death

When individual cells approach death, their division rates decrease (Fig. S6), and these senescence patterns are similar compared to the (chronological) senescence patterns (Fig. 1A, B) (Table S4 & Table S2).

Cell elongation rate for hours before death

The cell elongation rate does not drastically fall off when approaching death (no initial steep increase in cell elongation rate close to the time of death) (Fig. S7, Table S5). The senescence pattern is, at least for early and late daughters, less pronounced compared to that observed for chronological senescence (Fig. S3). Second generation daughters seem to reduce cell growth rates before death more substantially, but this reduction already starts a few hours before death and is not in line with terminal investment theories.

Cell size at division for hours before death

Cell size at division increased with chronological age, but mainly for early daughters (Fig. S3). One mechanism that might lead to such an increase in cell size at division is the formation of filamentous cells: cells that do continue to elongate but stop dividing. Such filamentation is usually seen as a stress response and increases mortality of the cell *(12, 43)*. Previous studies (conducted under different media and temperature than ours) have reported higher filamentation rates with increasing age *(12)*. Under our growth conditions, cells that entered a filamentation stage rarely recovered from that stage and did not return to a regular dividing smaller cell, though they not always stalled dividing. To test if such filamentous cells drive the chronological senescence pattern in size at division, we investigated the cell size for the hours before death. For early and late daughters, we detected an increase in cell size at division before death, but this increase is already initiated hours before the actual death and not a final increase in size due to filamentation (Fig. S7, Table S7).

Random deterioration model

Our random deterioration model builds on a LeBras type cascading failure model*(20)*. In such discrete state models, individuals increase from a current state i to a state $i+1$ at a rate proportional to i, and

mortality increases proportionally to state *i*. We can think of such states as accumulating damage, or model the reverse process, where an individual starts with some vitality and this vitality then decreases with increasing state *i* (random deterioration) *(21)*. In this study, we assume accumulating damage that stands symbolically for an unknown aging factor. These random deterioration models are mathematically closely linked to demographic frailty models that do not assume a stochastic stage progression among individuals, but rather heterogeneity of individual is defined by fixed frailty at birth *(14)*. Such frailty, an age independent mortality that follows a gamma distribution*(16)*, can be added to the classical models in demography, a Gompertz- model, which describes an age-dependent exponential increase in mortality. These models can also be extended by a Makeham term, an age-independent baseline mortality, which further improves model fit, at least for humans and various other complex species.

We first estimated parameters of such a Gamma-Gompertz-Makeham (GGM) model, $Zae^{bx}+c$ fitted to the survival data of the early daughters. *Z* is the random frailty variable that follows a gamma distribution across individuals. The distribution has a mean 1 and variance of σ^2. This definition of a gamma distribution with a mean of 1 implies that we have to set the scale parameter equal to the shape parameter of the gamma distribution. The rate of aging, *b*, is the same for all individuals, *x* determines the age in hours, *a* describes the baseline mortality of the Gompertz part of the model, and *c* describes the Makeham term, the age independent mortality.

We then transformed these estimates of the GGM model to a random deterioration model according to Yashin et al. *(14)*, making use of mathematical similarities between the GGM and random deterioration models.

μ_0=a+c, the probability of death at birth i.e. state *i*=0,

$\lambda_0 = \frac{b}{\sigma^2} - a$, the transition probability from state *i*=0 to state *i*=1,

$\lambda = b - \sigma^2 a$, the state transition probability between state *i* and *i+1*, for *i>0*

$\mu = \sigma^2 a$, the probability of death at state *i*, for *i>0*

Resulting estimates for early daughters were μ_0=0.056, $\lambda_0 = 0.178$, $\lambda = 0.598$, and $\mu = 0.00023$. Using these estimates for early daughters, we estimated the probability of observing an individual at state *i* at age *x*, *P(x,i)*,

$$P_i(x) = \begin{cases} P_0(0)e^{-(\lambda_0+\mu_0)x}, & i = 0 \\ \frac{P_0(x)}{i!}\left[\frac{\lambda - \lambda e^{-(\lambda+\mu)x}}{\lambda+\mu}\right]\prod_{k=1}^{i}\left(\frac{\lambda_0}{\lambda} + (k-1)\right), & i > 0 \end{cases}$$

We then built a matrix of $P(x, i)$ for which we limited the age, *x*, between 0 and 31 and the states were limited between 0 and 5000. The column sum of this matrix equals the survival probability at any given age *x* to age *x+1*.

Microsimulations of the random deterioration model

In order to simulate the (damage) state at death distribution we used a microsimulation. As a step-by-step calculation would take too long, we modelled the state at death distribution by drawing of a Poisson distribution with a rate of $\frac{1}{\mu_0 + \hat{\imath}\mu}$, where $\hat{\imath} = i + \frac{1}{\mu_0 + i\mu}$. In doing so, we estimated the expected state at death, rather than tracking individuals transitioning through damage states and their associated mortality risk as a step-by-step calculation would do. A step-by-step simulation would take a long time because individuals can easily end up in very high damage states (very long tailed distributions).

Estimating parameters for the late daughters

For the late daughters, we used the same state transition and survival parameters (μ_0=0.056, $\lambda_0 = 0.178$, $\lambda = 0.598$, and $\mu = 0.00023$) that we estimated for the early daughters. We did so because early and late daughter cells should biologically not be fundamentally different – aside of starting with different damage levels at birth. They should accumulate damage at the same rate and should experience mortality risk just based on their damage state. We assumed that the late daughters are born at the same stage, or a scaled version of the same stage, in which the mothers died, therefore let

$$\lambda_{0,late} = nint(s(\lambda_{0,early} + i\lambda))$$

$$\mu_{0,late} = nint(s(\mu_{0,early} + i\mu))$$

Where subscript *late* and *early* denotes late and early daughter estimates and $s \in (0,1)$ and $nint(.)$ is the nearest integer function. So based on the estimated damage state distribution of the mothers at death (early daughters), we also knew the damage state distribution at birth of the daughters (late daughters) [see below for optimally scaling this distribution]. Using the state transition probabilities of the early daughters and the probabilities of death, we estimated the survival of the late daughters. We also estimated the survival functions of cells that did not change their damage state with age. Each grey line in main text Fig. 2, describes such a fixed damage class survival function.

In order to determine the transmission fraction of accumulated damage between mothers (early daughters) and daughters (late daughters), we optimized the scaling of the mother state at death distribution (fraction of mother-daughter transmission) to the daughter age at birth distribution. The optimization was based on observed survival of the late daughters, by minimizing the squared deviations from the observed survival function. This optimal scaling factor was estimated at 7%.

Similar to the late daughters, we simulated the damage state distribution at birth, the damage state distribution at death, and calculated the matrix $P(x,i)$ for the second generation late daughters.

Supplementary material: Figures and Tables

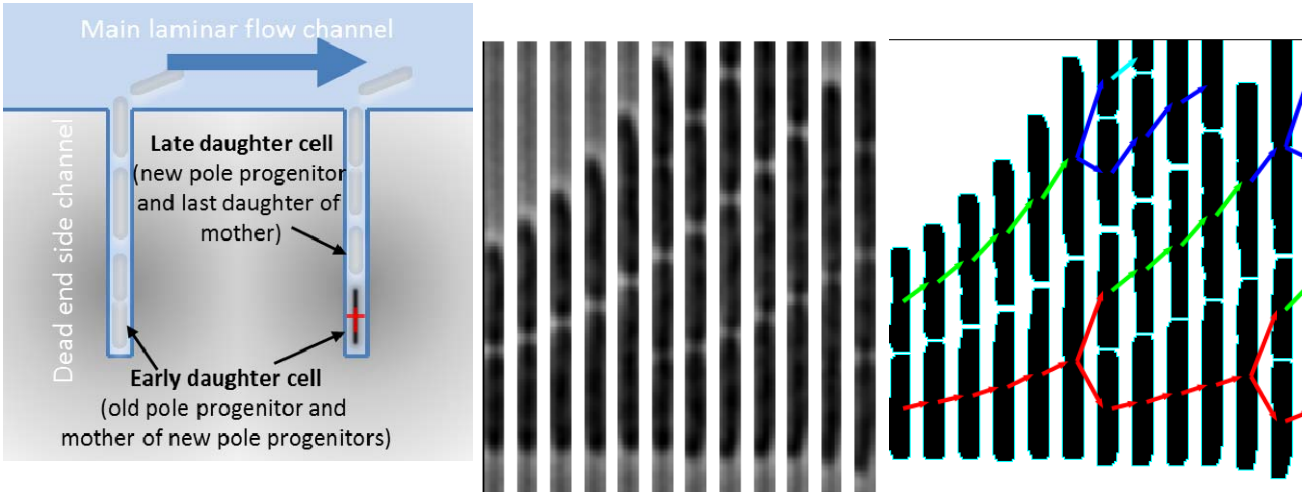

Fig. S1: Left panel: Overview sketch of the microfluidic device with dead-end side channels and the main laminar flow channel where the media is flushed through. The early daughter cells (founding initial loaded cells) are the bottommost cells of the dead end channels. Their daughter cells (new pole progenitor cells) are located closer to the main laminar flow channel. When the early daughter cell dies, its last daughter cell is then tracked throughout its life. We call these last cells late daughter cells. Second generation late daughter cells are then accordingly the last daughter cells produced by the first „cohort“ of late daughter cells. Centre and right panel: Time sliced (4 min intervals) side channel with initial loaded early daughter cell (old pole progenitor). Growth (cell elongation) and division can be tracked throughout their life as easily seen of the segmented cell lineages (right panel). The bottom cell (red cell) is the early daughter cell (old pole progenitor). See also Movie 1.

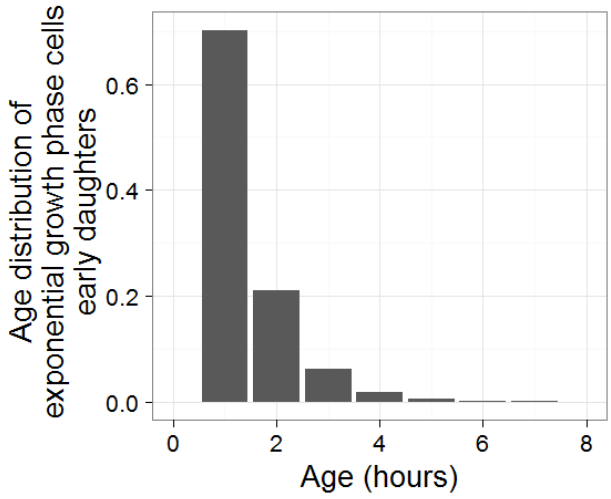

Fig. S2: Expected (stable) age distribution (in hours) of early daughters (initial loaded cells), estimated from a Leslie matrix parameterized with the demographic rates of the early daughter cells. Due to the theory of stable age populations, the distribution of the ages of the mothers of these early daughters should be exactly as the (stable) age distribution shown here of the initial loaded (early daughter cells) at the start of the experiments.

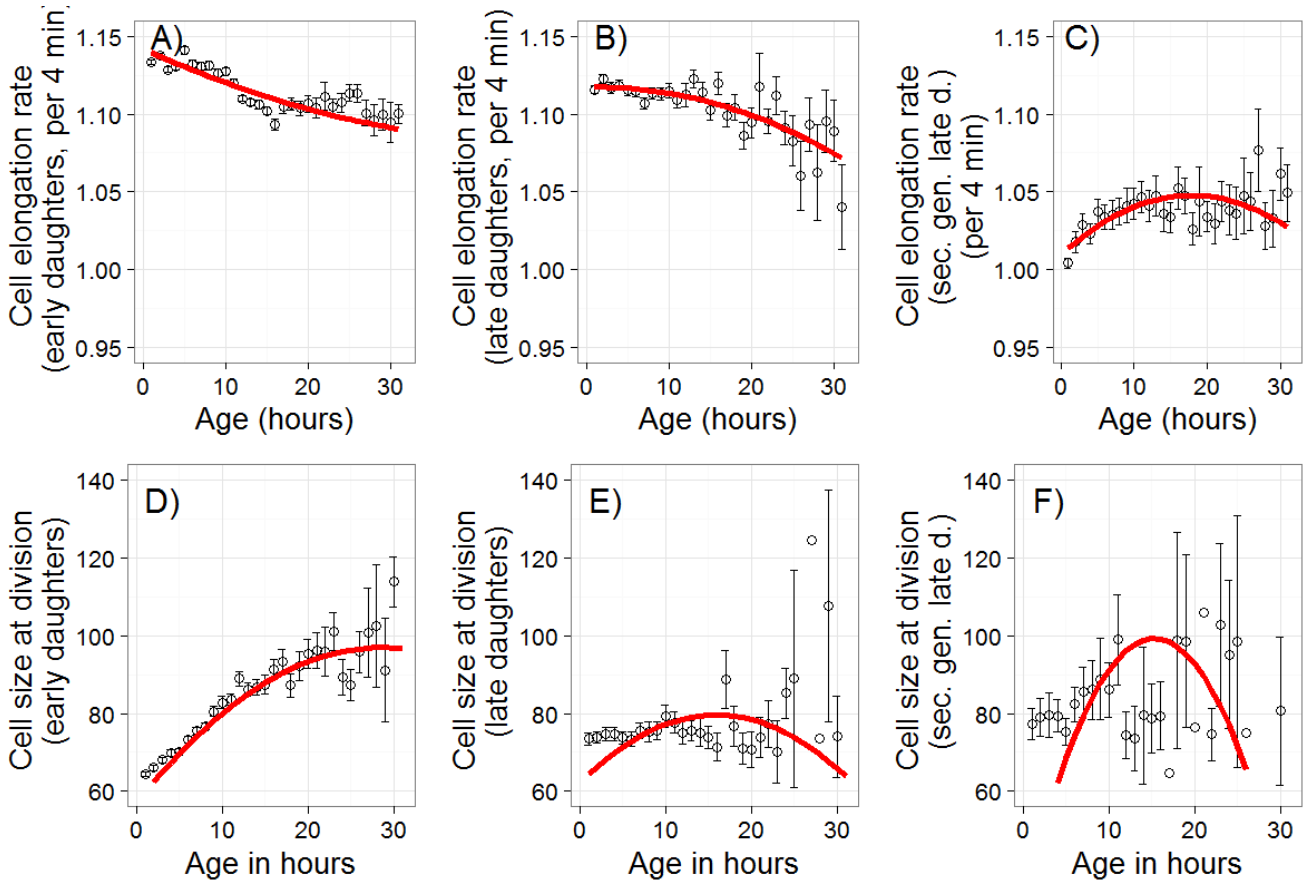

Fig. S3: A-C) Age-specific cell elongation rate (fractional elongation) and D-F) cell size at division (in pixels, 1pixel=0.064 µm) of the A&D) 516 early daughter cells, B&E) 516 late daughter cells, and C&F) 298 second generation late daughter cells. Means ± standard errors are plotted, red lines are based on model selection using information criteria (AIC) (Table S1).

Table S1: Model selection for age-specific cell elongation rates and cell size at division.

Cell elongation rates

Model	Slope±Std. Error	Quadratic term	AIC	ΔAIC
Early daughters				
Elongation rate ~interc. only			-21415	407
Elongation rate ~age	-0.002±0.0001		-21820	2
Elongation rate ~age+age^2	**-0.002±0.0002**	**-0.00002±0.00001**	**-21822**	
Late daughters				
Elongation rate ~interc. only			-10264	45
Elongation rate ~age	-0.00102±0.00016		-10304	5
Elongation rate ~age+age^2	**0.00013±0.00047**	**-0.000052±0.00002**	**-10309**	
Second generation late daughters				
Elongation rate ~interc. only			-4042.4	32.1
Elongation rate ~age	0.0014735±0.00029 59		-4065.1	10.4
Elongation rate ~age+age^2	**0.00429±0.00088**	**-0.00012±0.000035**	**-4074.5**	

Cell size at division

Model	**Slope±Std. Error**	**Quadratic term**	**AIC**	**ΔAIC**
Early daughters				
Size at division ~interc. only			53741	1378
Size at division ~age	1.72±0.04		52431	68
Size at division ~age+age^2	**2.797±0.135**	**-0.049±0.006**	**52362**	
Late daughters				
Size at division ~interc. only			28592	101
Size at division ~age	0.75±0.09		28525	34
Size at division ~age+age^2	2.204±0.259	-0.069±0.012	28491	
Second generation late daughters				
Size at division ~interc. only			8381.7	276.2
Size at division ~age	3.036±0.223		8215.9	110.4
Size at division ~age+age^2	**8.919±0.576**	**-0.293±0.027**	**8105.5**	

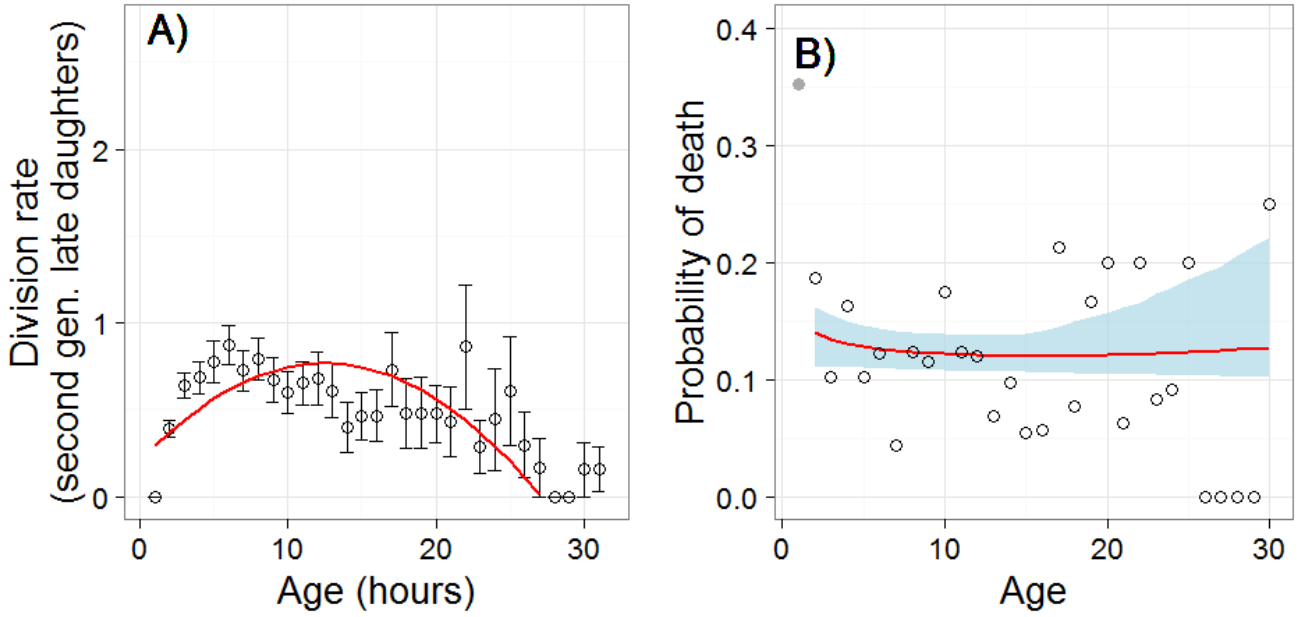

Fig. S4: Age-specific division rate (number of divisions per hour) (A) and age-specific hourly mortality rate (B) of the 298 second generation late daughters. For (A) means ± standard errors are plotted, for (B) means ± 95% Confidence Intervals are plotted. Red lines are based on model selection using information criteria (AIC) or the GGM model estimates (Table S2).

Table S2: Model selection division rate

Model	Slope±Std. Error	Quadratic term±StdE	AIC	ΔAIC
		Early daughters		
Divison rate ~intercept only			19663	24
Divison rate ~age	-0.011±0.002		19642	21
Divison rate ~age+age^2	**0.005±0.0078**	**-0.0007±0.0003**	**19638**	
		Late daughters		
Divison rate ~intercept only			12432	24
Divison rate ~age	-0.009±0.004		12428	20
Divison rate ~age+age^2	**0.039±0.011**	**-0.002±0.0005**	**12408**	
		Second generation late daughters		
Divison rate ~intercept only			5494	63.3
Divison rate ~age	0.009±0.004		5490.3	59.6
Divison rate ~age+age^2	**0.090±0.011**	**-0.004±0.0004**	**5430.7**	

Table S3: Model selection for age-specific mortality rates (q_x) of old (>19h) early daughters and old (>19h) late daughters, based on binomial models.

Model	Estimate±Std. Error	Quadratic term	AIC	ΔAIC
Mortality ~intercept only			95.79	6.09
Mortality ~cell type	**-0.591±0.211**		**89.7**	

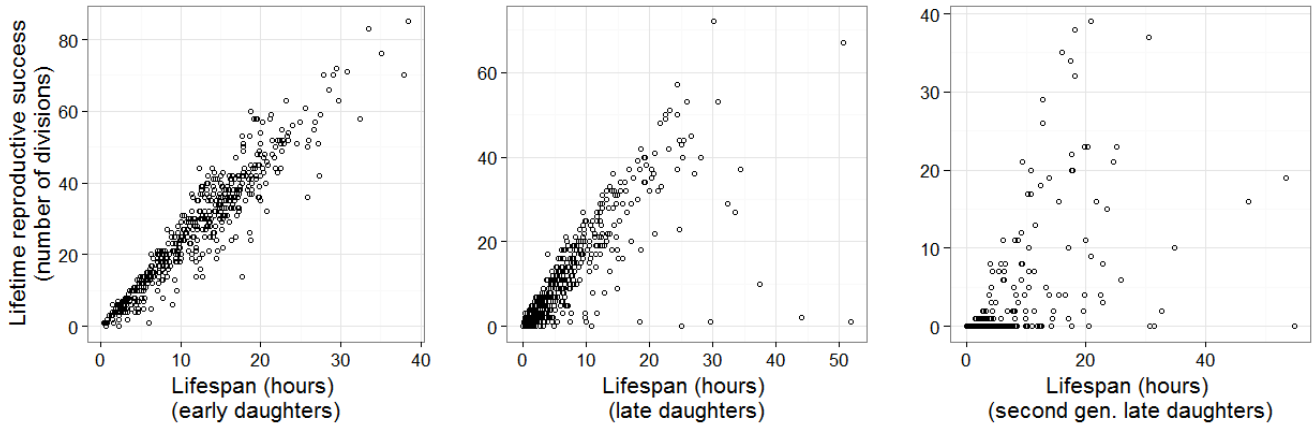

Fig. S5: Correlation between lifespan and the lifetime reproductive success (cumulative number of divisions an individual undergoes throughout its life) for left panel) the 516 early daughters, mid panel) the 516 late daughters, and right panel) the 298 second generation late daughters.

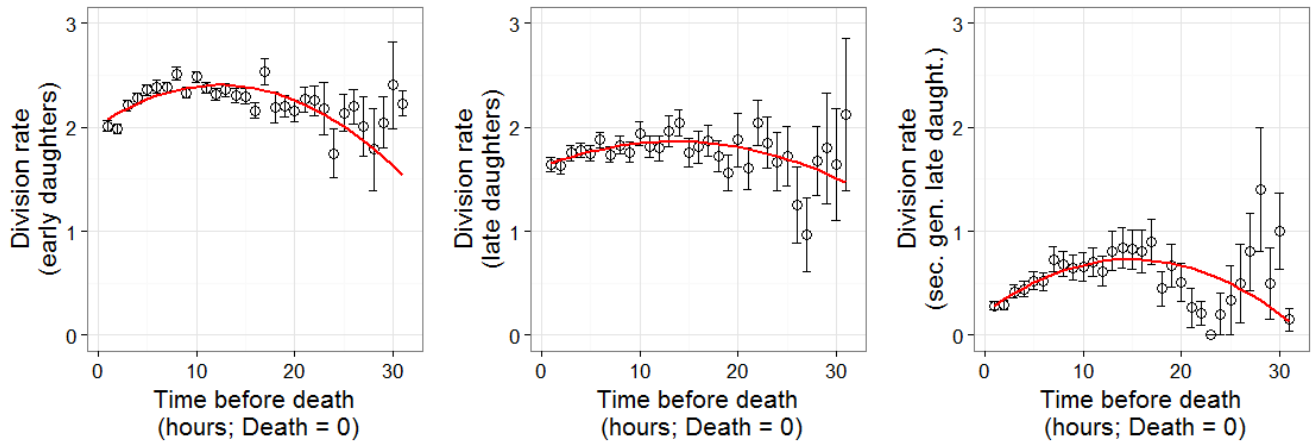

Fig. S6: Hourly division rate for hours before death [remaining life time] (death = time 0) for left panel the 516 early daughters cells, mid panel the 516 late daughters, and right panel the 298 second generation daughters. Means ± standard errors are plotted, red lines are based on model selection using information criteria (AIC) (Table S4).

Table S4: Model selection for division rate in reverse time (starting with age at death=0).

Model	Slope±Std. Error	Quadratic term	AIC	ΔAIC
Early daughters				
Division rate ~interc. only			19567	69
Division rate ~reverse time	0.006±0.002		19561	64
Division rate ~ reverse time + reverse time ^2	**0.062±0.0070**	**-0.002±0.0003**	**19497**	
Late daughters				
Division rate ~interc. only			12171	8
Division rate ~reverse time	0.006±0.003		12170	7
Division rate ~ reverse time + reverse time ^2	**0.036±0.017**	**-0.001±0.0004**	**12163**	
Second generation daughters				
Division rate ~interc. only			5474.5	47.8
Division rate ~reverse time	0.015±0.003		5456	29.3
Division rate ~ reverse time + reverse time ^2	**0.069±0.017**	**-0.002±0.0004**	**5426.7**	

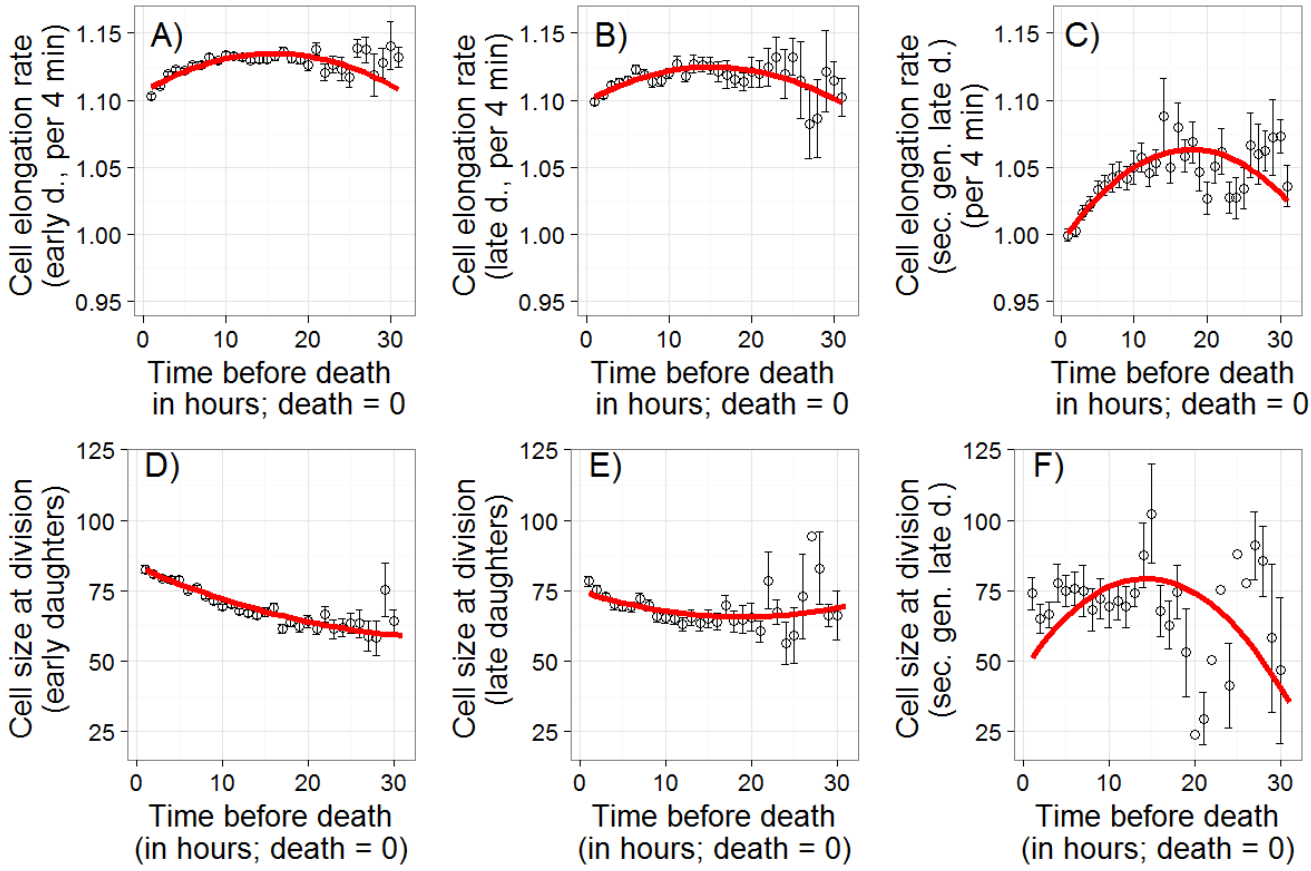

Fig. S7: (Fractional) Cell elongation rate and cell size at division (in pixels, 1pixel=0.064 µm) for hours before death (death = time 0) for A & D) the 516 early daughters, B & E) the 516 late daughters, and C & F) the 298 second generation late daughters. Means ± standard errors are plotted, red lines are based on model selection using information criteria (AIC) (Table S5).

Table S5: Model selection for cell elongation and cell size at division rate in reverse time (starting with age at death=0).

Model	Slope±Std. Error	Quadratic term	AIC	ΔAIC
Cell elongation (reverse time)				
Early daughters				
Elongation rate ~interc. only			-22138	250
Elongation rate ~reverse time	0.001±0.00009		-22288	100
Elongation rate ~ reverse time + reverse time ^2	**0.004±0.0003**	**-0.0001±0.00001**	**-22388**	
Late daughters				
Elongation rate ~interc. only			-10529	65
Elongation rate ~reverse time	0.001±0.0001		-10561	33
Elongation rate ~ reverse time + reverse time ^2	**0.003±0.0004**	**-0.0001±0.00002**	**-10594**	
Second generation late daughters				
Elongation rate ~interc. only			-4082.8	122.1
Elongation rate ~reverse time	0.003±0.0003		-4167.5	37.4
Elongation rate ~ reverse time + reverse time ^2	**0.008±0.0009**	**-0.0002±0.00003**	**-4204.9**	
Cell size at division (reverse time)				
Early daughters				
Size at division ~interc. only			53679	386
Size at division ~reverse time	-0.952±0.0486		53299	6
Size at division ~ reverse time + reverse time ^2	-1.337±0.145	0.018±0.006	53293	
Late daughters				
Size at division ~interc. only			28629	26
Size at division ~reverse time	-0.438±0.088		28606	3
Size at division ~ reverse time + reverse time ^2	**-0.990±0.258**	**0.026±0.011**	**28603**	
Second generation late daughters				
Size at division ~interc. only			8182.3	54.9
Size at division ~reverse	1.254±0.236		8156.6	29.2

time			
Size at division ~ reverse time + reverse time ^2	**4.531±0.627**	**-0.158±0.028**	**8127.4**

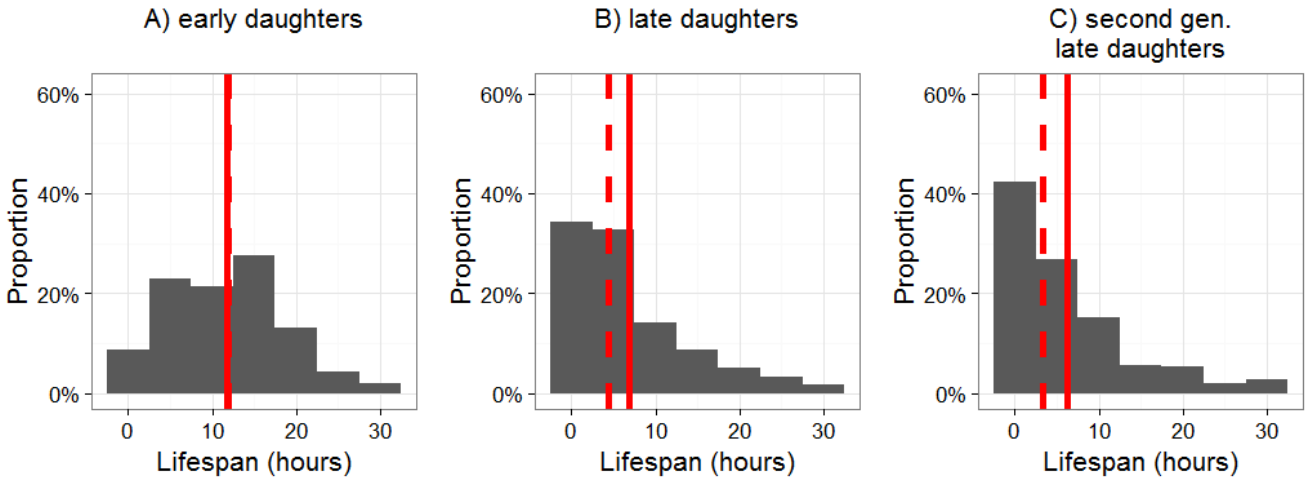

Fig. S8: Lifespan distribution (in hours) of isogenic *E. coli* cells grown under identical environmental conditions in a microfluidic device (Fig. S1). 1A – Founding early daughter cells (Median±stdev lifespan 12 ± 6.8 hours, Coefficient of Variation, CV 0.57) (N=298); 1B – Late daughters (last daughter) of the founding early daughters of 1A (Median±stdev lifespan 4.4 ± 7.0 hours, Coefficient of Variation, CV 1.03) (N=298); 1C – Second generation late daughters (last daughter of the late daughters of 1B; (Median±stdev lifespan 3.4 ± 7.1 hours, Coefficient of Variation, CV 1.14) (N=298). (Fig. S1 & S3). Hence, early daughters are the mothers of late daughters and grandmothers of second generation late daughters.

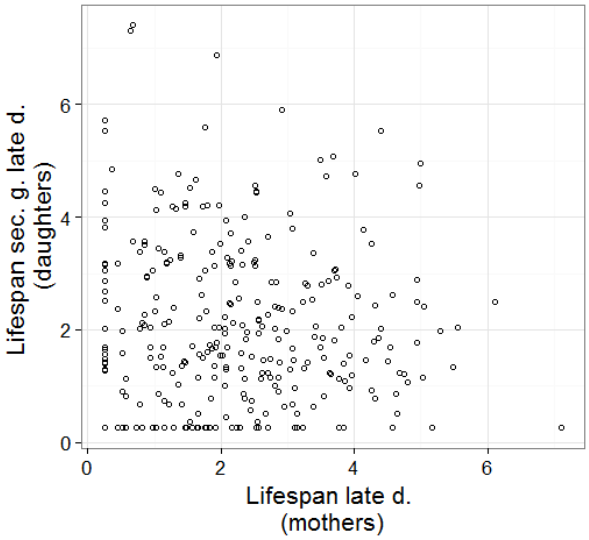

Fig. S9: Correlation between lifespan (Square root-transformed) of the 298 late daughters [mothers] versus the lifespan of their last daughter cell, the second generation late daughters (Table S6).

Table S6: Model selection for correlation between lifespan (Square root transformed, Gaussian error)

Model	Slope	Std. Error	T value	p-value	AIC	ΔAIC
Early daughters [516 mothers] and daughter cell (last daughter of early daughter)						
sqrt(Lifespan Daughters) ~ sqrt(Lifespan mothers)	-0.10	0.05	-1.8	0.07	1774.1	
sqrt(Lifespan Daughters) ~ intercept only					1775.5	1.3
Late daughters [mothers 298] and second generation late daughters (last daughter cell produced by late daughters)						
sqrt(Lifespan Daughters) ~ sqrt(Lifespan mothers)	- 0.09	0.06	-1.55	0.12	1061.1	
sqrt(Lifespan Daughters) ~ intercept only					1061.5	0.4

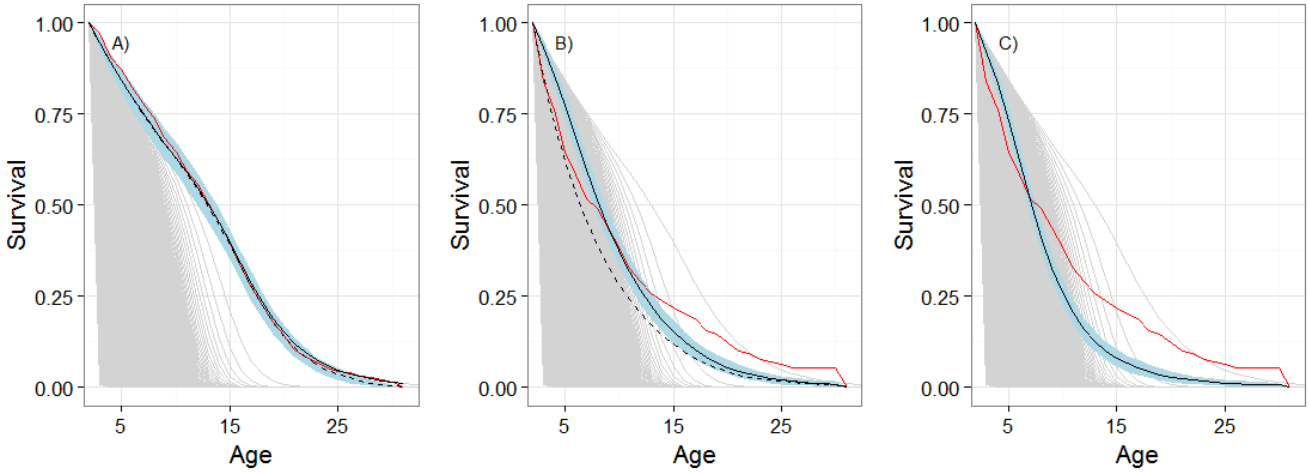

Fig. S10: Observed population level survival curve (red line), GGM simulated survival curve with symmetric damage transmission (hatched black line) as well as GGM simulated survival curve with asymmetric damage transmission of 7% (solid black line ± 95% CI in blue) for early (A), late (B) and second generation late daughters (C). Graphs A & B are identical to Fig. 1C & D. Thin grey lines in depict expected survival curve of cells with different fixed damage state. That is, for instance, the outermost thin grey line in B depicts the survivorship curve of a hypothetical cohort that starts without damage and never accumulates any damage. The most left survival curve illustrates the low survival of cells that were born with maximum damage level of 5000.

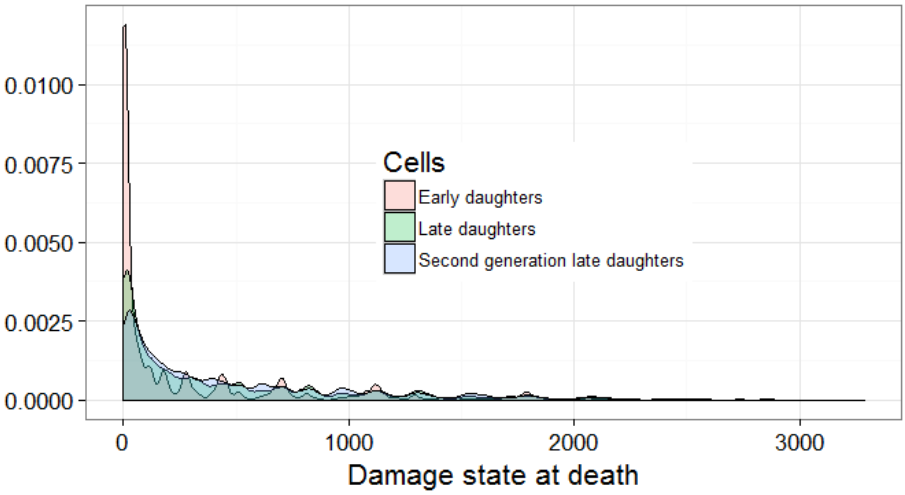

Fig. S11: Density distribution of damage state at death of early daughters, late daughters, and second generation late daughters. Most cells die with little accumulated damage. Note, the not so smooth tails of the distributions are a result of drawing from a Poisson distribution in our simulations.

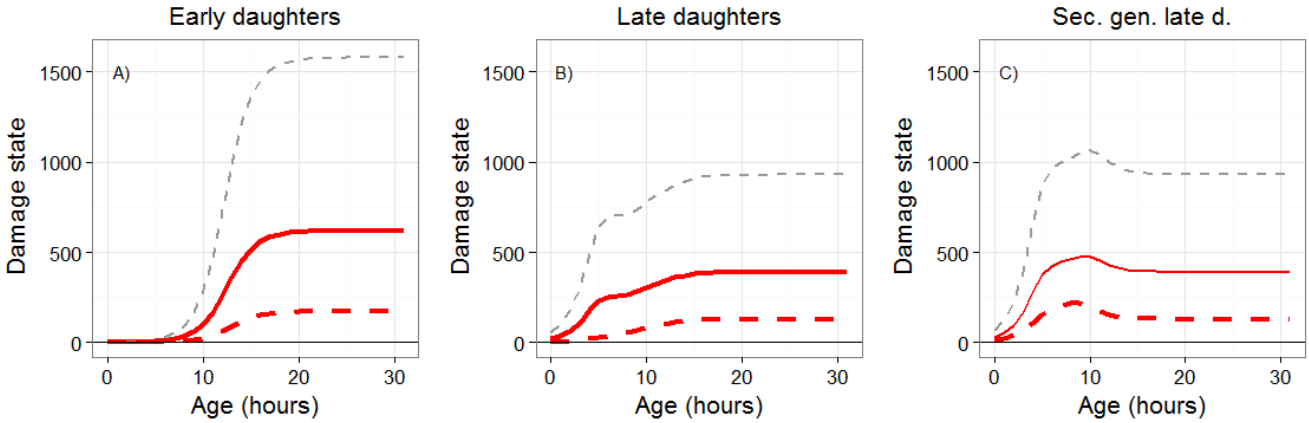

Fig. S12: GGM model results: mean (red solid line, + SD grey hatched lines) and median (red hatched line) damage state with increasing age for early daughter cells (A), and late daughter cells (B) and second generation late daughter cells (C). Panel A & B are identical to Panel Fig. 1A, B.